

Anisotropic particle motion in optical landscapes modeled via the T-matrix optical scattering approach

Brandon L. Conover and Michael J. Escuti

North Carolina State Univ, Dept Electrical & Computer Engineering, Raleigh, NC (USA)

ABSTRACT

Optical manipulation of nano- and micro-scale particles via optical tweezers and optical landscapes continues to be of great interest in several fields, reflected by the myriad experimental pursuits suggesting selective and parallel control over particles of anisotropic shape (blood cells, nanorods, etc.). Our work here approaches the goal of a complete model of these phenomena by means of optical scattering principles and, specifically, the T-matrix method. Here we describe the salient features of our model, which tends toward a complete and consistent modeling scheme for determining the behavior of dielectric, polarizable, mesoscale particles of anisotropic shape in arbitrary intensity gradients. We explore forces and torques caused by periodic optical landscapes as well as torques induced by the polarization orientation of the electric field.

Keywords: Optical Trapping, Optical Landscapes, T-Matrix Method, Optical Scattering

1. INTRODUCTION

Trapping and manipulation of nano- and micro-scale particles within a microfluidic environment continues to be of great interest to several scientific communities. For example, the field of microfluidic lab-on-a-chip would be greatly enhanced by having access to accurate and efficient mechanisms for sorting chemical and biological colloids. Broadly, there are two techniques for colloidal separation: extrinsic, requiring external identification of particles (e.g., FACS), and intrinsic, in which properties inherent to the particles themselves (e.g., size, refractive index) are exploited. Extrinsic methods can add time and cost to the design of new assays in addition to being invasive to the particles themselves. Leading the charge toward intrinsic-based techniques are dielectrophoretic (DEP)^{1–5} and optical field^{6–10} sorting systems. These incorporate continuous fluid flow and generally easy reconfiguration means for efficient particle sorting in theoretical terms, experimental observations, or both.

While the majority of these techniques and others like them consider spherical beads and mammalian cells as their particles of interest, they rely on properties such as surface conductance⁵ or particle size,^{7,10} and not on the *shape* of the particle. Neglecting particle shape when analyzing experimental results of sorting does not negatively impact physical results (e.g., a given system that sorts particles regardless of the means still sorts the particles!). However, developing a complete theoretical model of colloidal motion based on DEP or optical fields would almost certainly be incomplete without some incorporation of particle shape.

Due to the absence of fabricated electrodes and their on-the-fly reconfiguration abilities, optical fields are affordable and versatile engines for optical sorting systems. However, no satisfactory theoretical model has been presented that addresses all aspects of optical manipulation and sorting simultaneously. Many current models and measurement schemes focus on single aspects of the system: periodic optical landscapes that exert optical forces on spherical particles,^{6,11,12} Gaussian intensity fields that transfer optical torques to ellipsoidal particles,^{13,14} etc. For the model to be complete, it must consider dielectric particles of arbitrary size, shape, and composition; it must address both optical forces and optical torques; and, when considering particle motion over time through a fluid, it must allow for an arbitrary fluid flow—all within the boundaries of optical trapping and microfluidic environments.

In pursuit of such an all-encompassing model, we have developed and present here two order-of-magnitude approximations of the response of isotropic dielectric particles of spheroidal shape in optical intensity fields. The first, previously presented¹⁵ and termed the form-factor model, is based on the polarizability and form factor of

Correspondence should be addressed to: mjescuti@ncsu.edu, +1 919 513 7363

the particles and their interactions (i.e., optically-induced forces and torques) with the optical fields. The second, termed the T -matrix model, is based on the linear scattering of the electric fields at the surfaces of the particles. We use the T -matrix method to calculate the amplitude scattering matrix in the far-field¹⁶ thus allowing us to transform the incoming electric fields (incident plane waves) into the outgoing electric fields (scattered spherical waves). The Maxwell stress tensor (MST) is then employed around the particle to find the optically induced gradient forces (in-plane), scattering forces (out-of-plane), and torque. The incident fields we consider in both models are primarily one- and two-dimensional periodic interference landscapes formed by simple holography without the need for high N.A. objective lenses holographic elements. However, the generality of our models allows for a large range of incident radiation to be applied.

This work intends to provide an overview of the development of the form-factor model and a more in-depth treatment of the T -matrix model, each as an independent entity. Several results of the T -matrix model will be provided and some comparison between the two models will be discussed. We intend for our work to show that the form-factor model continues to be a more straightforward implementation than comparable models and applicable to numerous trapping and sorting systems. We provide the T -matrix model as an independent tool for analyzing particle motion and, finally, as verification and furtherance of the form-factor model. For example, the T -matrix model is capable of calculating the scattering forces as well as torques on particles of shape as induced by their angular separation from the incident electric field polarization orientation—both of which are absent in the form-factor model. We will show that these effects are significant and should be considered by any complete model.

2. THE T -MATRIX MODEL

The forces on our particles within optical landscapes include gradient forces, acting in the transverse plane, and scattering forces (radiation pressures) acting most appreciably in the direction of light propagation. As will be discussed below, our form-factor model assumes the scattering forces to be negligible in comparison to the gradient forces and does not explicitly consider them. Furthermore, polarization effects are neglected. In the interest of forming a complete and accurate model, we have developed a second model of particle motion accounting for both the gradient and scattering forces and polarization effects. It is based on solving the MST using scattered electric fields in the far-field regime. Such fields may be found by employing the T -matrix method.

The T -matrix method has been effective in analyzing the forces and/or torques on particles suspended in a Gaussian optical trap^{13,17,18} and has been well defined in more general terms^{16,19} for analyzing far-field electromagnetic scattering. We employ it here in analyzing the forces and torques on isotropic, spheroidal particles within periodic optical landscapes. The method effectively provides exact solutions to Maxwell's equations—necessary for accurate modeling of particles on the order of the illuminating wavelength—via expansion of the incident and scattered fields as vector spherical wave functions. The expansion coefficients of the scattered field are related to those of the incident field through a linear transformation matrix, i.e., the T -matrix. Forces and torques on particles residing within the fields may then be found using the Maxwell stress tensor. We have chosen the T -matrix method due to the availability of precision computer code provided and described by Mishchenko et al¹⁹ and for its flexibility in analyzing groups of particles, various media, and a large range of particle sizes—all areas into which we intend to expand our model(s). Because of the aforementioned availability of information regarding the T -matrix method, it will only be briefly outlined here while highlighting the adaptations made for our model.

2.1 Electric Fields, Particle Orientation, and the T -Matrix Method

We begin in the laboratory reference frame by defining the incident electric field with the time-harmonic factor, $\exp(-i\omega t)$ assumed and suppressed. Additionally, all magnetic fields are neglected as we will only consider non-magnetic particles. Following Escuti and Crawford,²⁰ the m 'th incident wave in phasor notation (Fig. 1(a)) is defined as

$$\mathbf{E}_m^{inc}[\mathbf{r}] = E_m^{inc} \exp(i\mathbf{k}_m \cdot \mathbf{r} + i\delta_m) \mathbf{e}_m, \quad (1)$$

where E_m^{inc} is the real amplitude, $\mathbf{r} = (x, y, z)'$ is the position vector connecting the origin of the laboratory reference frame to the observation point, \mathbf{k}_m is the propagation vector, and δ_m is the absolute phase. Note that

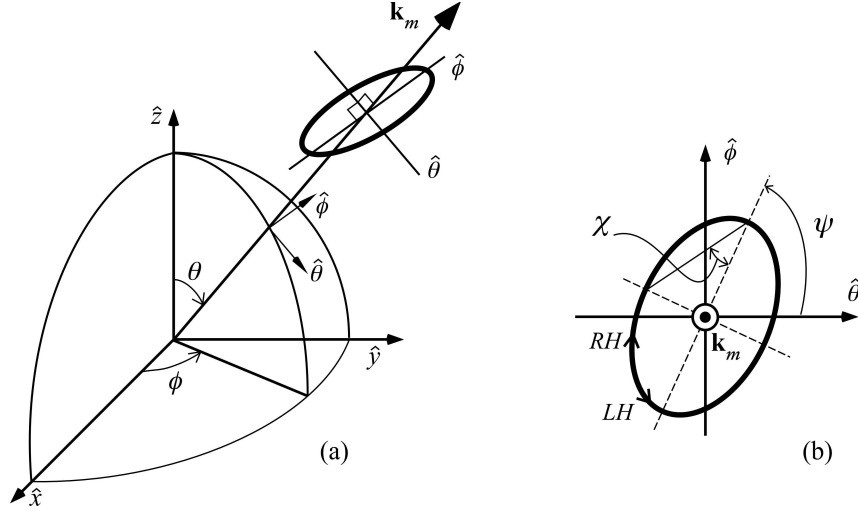


Figure 1. Coordinate System and Polarization Conventions. (a) Propagation angles. (b) Polarization angles.

the symbol ' corresponds to the simple vector transpose. As will be convenient when describing our particles, we use the spherical coordinate system to express \mathbf{k}_m such that

$$\mathbf{k}_m = \frac{2\pi}{\lambda} (\cos \phi_m \sin \theta_m, \sin \phi_m \sin \theta_m, \cos \theta_m), \quad (2)$$

where θ_m and ϕ_m are the polar and azimuthal angles, and λ is the wavelength of the incident radiation. The polarization of the m 'th wave can be described in terms of the orientation and ellipticity angles, ψ_m and χ_m , as shown in Fig. 1(b) using the standard convention for handedness. The ranges of the polar, azimuth, orientation, and ellipticity angles are $0 \leq \theta \leq \pi$, $-\pi < \phi \leq \pi$, $0 \leq \psi < \pi$, and $-\pi/4 \leq \chi \leq \pi/4$. As per standard convention, $(\chi = 0, \psi = 0)$ corresponds to transverse-magnetic (TM) polarization and $(\chi = 0, \psi = \pi/2)$ corresponds to transverse-electric (TE) polarization. With polarization information, we can now define the spherical components of the m incident electric fields in the laboratory reference frame interfering at the origin as

$$E_{m\theta}^{inc} = E_m^{inc} \exp(i\delta_m) (\cos \psi_m \cos \chi_m + i(-\sin \psi_m \sin \chi_m)) \quad (3a)$$

$$E_{m\phi}^{inc} = E_m^{inc} \exp(i\delta_m) (\sin \psi_m \cos \chi_m + i \cos \psi_m \sin \chi_m). \quad (3b)$$

Assuming linear boundary conditions on our particle, Maxwell's equations allow us to express the scattered electric field linearly in the incident electric field. This is achieved via a 2×2 amplitude matrix (aka scattering matrix, T -matrix) defined in the laboratory reference frame that transforms the electric field vector components of the incident wave into the corresponding components of the scattered wave. In the far-field region, when the observation point is a distance R much greater than $\lambda/2\pi$ away from the particle, the n 'th scattered wave becomes spherical and may be written as²¹

$$\begin{bmatrix} E_{n\theta}^{sca} \\ E_{n\phi}^{sca} \end{bmatrix} = \frac{\exp(ikR)}{R} \mathbf{S} \begin{bmatrix} E_{m\theta}^{inc} \\ E_{m\phi}^{inc} \end{bmatrix}, \quad (4)$$

where \mathbf{S} represents the 2×2 amplitude matrix. This amplitude matrix depends on the directions of the incident and scattered beams and on the size, morphology, and relative permittivity of the particle. Furthermore, since the particle must also exist in the laboratory reference frame, \mathbf{S} will depend on the orientation of the particle. Because we will focus on rotationally symmetric particles, it will be easiest to align the axis of rotation along the \hat{z} -axis of a locally defined particle reference frame, transformed to the laboratory frame by the well-known Euler angles of rotation, α and β . Symmetry allows γ to be zero.

The calculation of \mathbf{S} is performed primarily by the double precision T -matrix code for nonspherical particles in a fixed orientation from Mishchenko et al.¹⁹ We have modified this code to provide a scattering matrix at any given number of points on a sphere surrounding the particle. Our general procedure for obtaining the scattered fields is as follows:

1. Define parameters of the particle such as Euler angles, dimensions, composition, shape, etc.
2. Describe a sphere with radius R such that $kR \gg 1$, a criterion for far-field scattering. The sphere surrounds the particle and shares its origin. Using iterative functions of common computer programs, the surface of the sphere is then divided into n equal-surface-area segments having polar and azimuthal coordinates (θ, ϕ) centered at each segment. These define the points at which the scattering matrices will be calculated.
3. Define any number m of incident electric field vectors interfering at the laboratory frame origin using the coordinate system as defined in Fig. 1.
4. Using the T -matrix code, calculate the scattering matrix at each coordinate pair (θ, ϕ) .
5. Transform the incident electric field vectors into m scattered electric field vectors at each of n points around the sphere using Eq. 4.

2.2 Force, Torque, and The Maxwell Stress Tensor

Once the scattered electric field vectors have been calculated around the particle, a simple superposition of the field vectors at each point must occur. This accounts for the interference that is created by the m incident beams interfering at the laboratory frame origin. This is done after calculation of the amplitude matrix and scattered field vectors merely for simplicity. To perform the component-wise summation of these vectors, we must first transform the scattered field vectors from spherical coordinates to cartesian using a 3×2 transformation matrix as follows:

$$\mathbf{E}_n^{sca}[\mathbf{r}] = \begin{bmatrix} E_{nx}^{sca} \\ E_{ny}^{sca} \\ E_{nz}^{sca} \end{bmatrix} = \begin{bmatrix} \cos \theta \cos \phi & -\sin \phi \\ \cos \theta \sin \phi & \cos \phi \\ -\sin \theta & 0 \end{bmatrix} \begin{bmatrix} E_{n\theta}^{sca} \\ E_{n\phi}^{sca} \end{bmatrix}, \quad (5)$$

where $\mathbf{r} = (x, y, z)$ and (θ, ϕ) are the spherical coordinate components of the vector normal to the respective segment on the sphere. Superposition is performed via component-wise summation of all scattered electric field vectors.

As our goal is to use these fields to solve for the various forces and torques on our particle of interest, the full Maxwell stress tensor must be computed at each of n points using the cartesian coordinate system. This involves writing the vector summation of the incident and scattered fields as \mathbf{E}^{tot} and to then compute the MST at each of n points using the cartesian coordinate system. The MST is commonly represented by¹⁸

$$\langle \overleftrightarrow{\mathbf{T}}_n[\mathbf{r}] \rangle = \frac{\epsilon_m \epsilon_0}{2} \Re \left\{ \mathbf{E}_n^{tot}[\mathbf{r}] \mathbf{E}_n^{tot*}[\mathbf{r}] + \frac{1}{2} |\mathbf{E}_n^{tot}[\mathbf{r}]|^2 \overleftrightarrow{I} \right\}, \quad (6)$$

where $\mathbf{E}\mathbf{E}^*$ is a dyadic product, \overleftrightarrow{I} is the unit tensor, and angle brackets represent a time average of harmonic fields. Both the MST and the unit tensor are of rank two. The net force on the particle can then be found by integrating the product of $\overleftrightarrow{\mathbf{T}}$ and the unit vector at each of n points over the surface of the sphere enclosing the particle:

$$\mathbf{F}[\mathbf{r}] = \int \langle \overleftrightarrow{\mathbf{T}}_n[\mathbf{r}] \rangle \cdot \hat{\mathbf{n}} dA, \quad (7)$$

where $\hat{\mathbf{n}}$ is the unit vector on the sphere in cartesian coordinates and dA is the infinitesimal area which, in this case, is the area of each of n segments. Knowing the outgoing far-field scattered field components, we can write this force in terms of their complex amplitudes¹⁷

$$\mathbf{F}[\mathbf{r}] = \frac{\epsilon_m \epsilon_0}{2} \int (E_{\theta}^{sca} E_{\theta}^{sca*} + E_{\phi}^{sca} E_{\phi}^{sca*}) \hat{\mathbf{n}} dA, \quad (8)$$

where the integrand is the rate of transfer of linear momentum per unit area. Similarly, the torque on the particle may be written in terms of the MST as

$$\mathbf{M}[\mathbf{r}] = - \int \mathbf{r} dA \cdot [\langle \vec{\mathbf{T}}_n[\mathbf{r}] \rangle \times \mathbf{r}], \quad (9)$$

and in simplified fashion as

$$\mathbf{M}[\mathbf{r}] = \frac{ic\epsilon_m\epsilon_0}{2\omega} \int (E_\theta^{sca} E_\phi^{sca*} - E_\theta^{sca*} E_\phi^{sca}) \hat{\mathbf{n}} dA, \quad (10)$$

where the integrand is the rate of angular momentum per unit area, c is the speed of light in a vacuum and ω is the angular frequency. It is interesting to note that in the simplified equations for force and torque, only the scattered fields need to be considered, rather than the total fields as is the case with the full MST description. Part of this simplification arises from a consideration of the polarization changes—or the lack thereof—brought on by the particle. Both approaches are valid and our model implements the simplified equations.

3. IMPLEMENTATION OF THE T -MATRIX MODEL

The following sections will explore the results of implementing the T -matrix model with spherical and spheroidal particles within plane wave radiation and optical landscapes, i.e., periodic optical interference potential landscapes. For consistency, some parameters are the same for all results. The relative refractive index is defined as

$$n_r = \frac{n_p}{n_m}, \quad (11)$$

where n_p and n_m are the refractive indices of the particle and of the medium, respectively. Throughout this work, we use $n_r = 1.15$ and we normalize results to the incident wavelength. An electric field magnitude of 10^6 V/m, roughly corresponding to an intensity magnitude of 10^9 W/m², is employed in an effort to match probable laboratory laser systems. However, this could also be normalized out without adversely affecting trends within the results.

Our spheroid of interest is a prolate dielectric particle with rotational axis semi-diameter (a) equal to the radius of our sphere of interest and twice the length of the orthogonal axes' semi-dimeters ($b = c$). While its angle between the \hat{x} - and \hat{y} -axes may change according to the orientation angle Ω corresponding to the Euler angle α , its rotational axis will always be in the $\hat{x} - \hat{y}$ plane, achieved by Euler angle $\beta = 90^\circ$. As polarization is important to this model, we follow the convention in Fig. 1(b) for linearly polarized light, setting χ always to zero and ψ to 90° (TE polarized) except where noted. For torque, we use the convention that a positive torque about the axis of propagation, the \hat{z} -axis, is in the clockwise direction when looking down the positive axis direction.

Finally, the reader should note that our model considers only plane waves in its current implementation. However, it is capable of any relevant input radiation described in terms of electric fields. For example, Gaussian beams could be considered by describing the incident radiation as a sum of several plane waves.

3.1 Single Plane Waves

Radiation consisting of a single plane wave propagating along the positive \hat{z} -axis is capable of transferring linear momentum to both spheres and non-spheres. This may also be referred to as radiation pressure. Eq. 8 allows for calculation of this force in terms of the scattered field. Due to the cross-sectional area and shape of various particles, total force may vary for the same incident field. Such a result is evident in Fig. 2(a) in which the scattering force on both a sphere and a prolate spheroid is plotted against the normalized size of the particle. Because the scattering force is proportional to the cross-sectional area of the particle, the result here is expected. The sphere has a radius equal to the rotational semi-diameter of the prolate particle, resulting in a larger cross-sectional area and a larger scattering force.

Because the T -matrix model considers polarization, a single plane wave is also capable of transferring angular momentum to particles of anisotropic shape. Such a particle will align in a minimum energy configuration in an incident field. For a single plane wave, this is parallel to the orientation of the electric field polarization. Fig. 2(b)

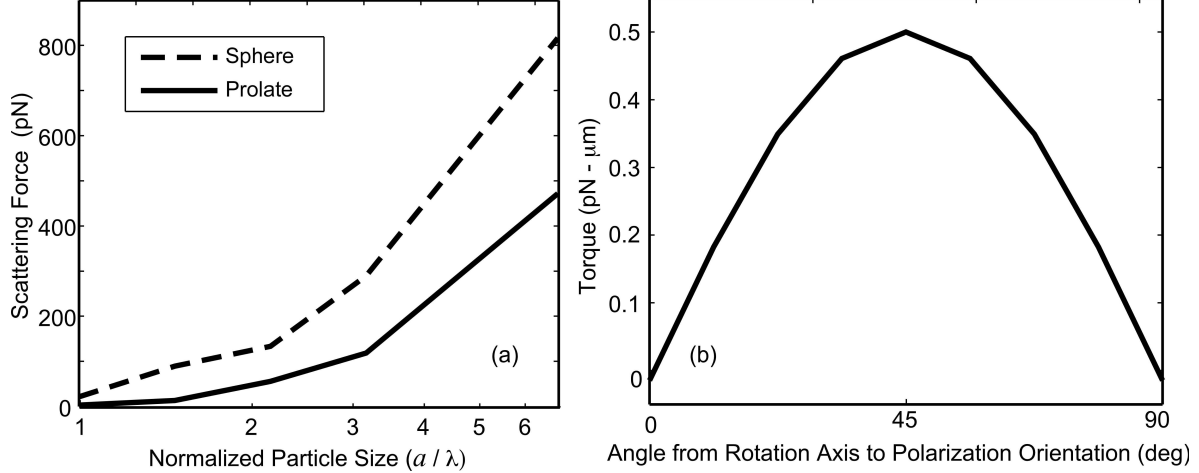


Figure 2. Forces and Torques Produced by a Single Plane Wave. (a) Scattering force on a sphere and a prolate spheroid of varying normalized size. (b) Torque on a prolate spheroid about the \hat{z} -axis. The torque acts to align the particle's rotational axis with the orientation of the electric field polarization.

represents such a situation. The torque about the \hat{z} -axis on a prolate spheroid acts to align the rotational axis with the polarization direction. Due to symmetry, the total torque on a sphere is always zero.

The scattering force will remain appreciable for any number of incident beams or plane waves, always acting to “push” the particle in the direction of propagation. The impact of the polarization-induced torque will always be present but may be overcome by gradient forces acting orthogonal to the propagation direction as will become apparent in the following section.

3.2 Interference of Two Plane Waves (Optical Landscapes)

Radiation consisting of more than one plane wave propagating at some orientation (θ, ϕ) as indicated in Fig. 2(a) will produce an interference pattern (optical landscape) with a grating pitch, Λ , in the plane orthogonal to the total vector direction of the incident waves. For our purposes, this grating pitch will be in the $\hat{x} - \hat{y}$ plane, parallel to the rotational axis of the prolate particle. Because of its symmetry, the orientation with respect to a sphere is the same regardless of propagation directions.

The 1D optical landscape created by two plane waves varies only in the \hat{x} -direction so that $I[x]$ is symmetrical in the \hat{y} -direction. Such is represented as

$$I[x] = I_0 \left(1 + \cos \left(\frac{2\pi}{\Lambda} x \right) \right). \quad (12)$$

The polar angle of the incident waves is related to the grating pitch by

$$\theta = \sin^{-1} \left(\frac{\lambda}{2\Lambda} \right), \quad (13)$$

where λ is the incident wavelength. We will consider only two incident plane waves where $\theta = \theta_1 = \theta_2$, $\phi_1 = 0^\circ$, and $\phi_2 = 180^\circ$, resulting in a one-dimensional optical landscape as described by Eq. (12). We will refer to the areas of constructive interference as bright fringes and to the converse areas as dark fringes. Our convention is such that a bright fringe will always occur at $x/\Lambda = 0$ and a dark fringe at $x/\Lambda = 0.5$.

3.2.1 Gradient Force

The gradient forces experienced by a particle in this system are represented in Fig. 3. A positive gradient will cause the particle to be drawn in the positive \hat{x} -direction. In general, we find with this model and with the form-factor model to be later discussed, that the gradient force will act to draw the particle toward the closest

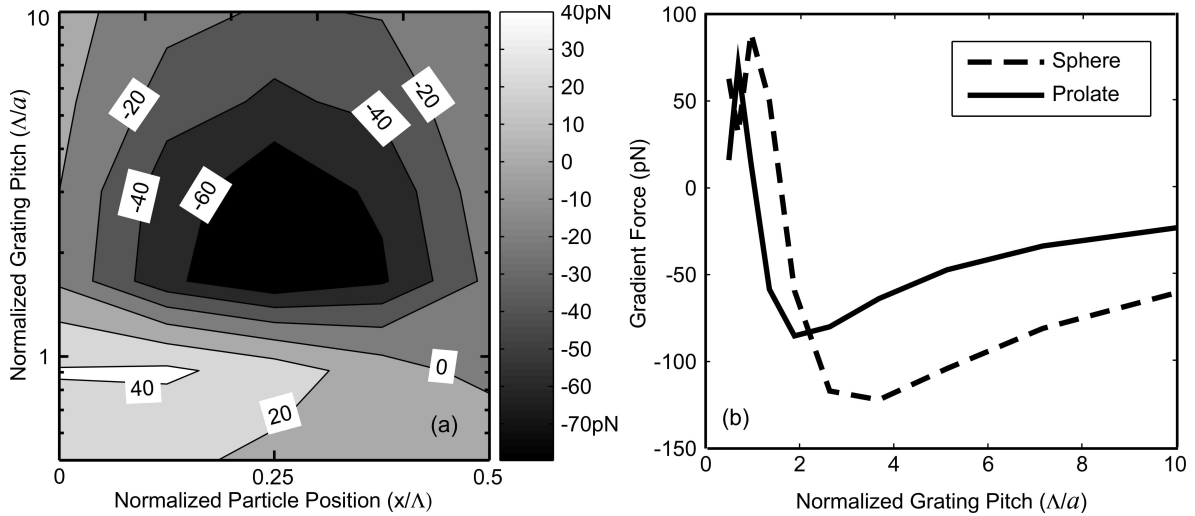


Figure 3. Gradient Force Induced by an Optical Landscape. (a) Contour plot of the gradient force on a prolate spheroid. Both the normalized grating pitch and particle position are varied. (b) Gradient force on a sphere and a prolate spheroid. The position is set to $x/\Lambda = 0.25$, halfway between a bright and dark fringe.

bright fringe. A particle located at a bright fringe is in a minimum energy configuration and a stable equilibrium. A particle located at a dark fringe is in a non-stable equilibrium state and will be displaced by any perturbation.

We conclude from Fig. 3(a) that the greatest negative gradient force will occur at the midpoint between a bright and dark fringe for a particle semi-diameter between $a = \Lambda/2$ and $\Lambda/4$. As expected, for a particle placed to the positive side of a bright fringe, the gradient force on the particle will be toward the origin.

Fig. 3(b) is the gradient force on both particle types at the midpoint, $x/\Lambda = 0.25$, for varying grating pitch. When the pitch is small relative to the particle, several bright fringes are present within the dimension of the particle. The gradient force will still act in the direction of the nearest bright fringe, in this case the positive direction. However, when the grating pitch is larger than the particle dimension, the gradient force is restorative toward the origin. At large Λ/a , the intensity can be approximated as linear near the midpoint. As Λ/a continues to increase, the slope of the intensity decreases, resulting in a gradient force on the particle decreasing toward zero. Similar to the case of a single incident wave, the total force on the sphere is greater than on the prolate particle yet the trend is still present.

3.2.2 Scattering Force

The scattering force is still present in our system regardless of the number of incident waves, because we are explicitly modeling an optical landscape that is not created with any high numerical-aperture objectives. In fact, the scattering force can be several orders of magnitude greater than the gradient force. This is evident in Fig. 4(a) in which the scattering force on a prolate particle varies between 100 – 1200 pN whereas, for the same system, the largest gradient force experienced is ≈ 100 pN. This has important implications in an experimental setting in that the particles are more likely to be propelled in the direction of beam propagation than they are to be drawn toward bright fringes in the plane of the grating pitch. From our analysis, it is clear that the scattering force must be counteracted or otherwise eliminated in order to manipulate particles in the optical landscape plane.

Fig. 4(b) compares the scattering force on the two particle types. Most interesting to note is the intersection of scattering force magnitude on a prolate particle when $\Lambda \approx a$, regardless of the position. This occurs because in this case, the same number of bright fringes lies within the dimension of the particle, resulting in the same total scattering force. Increasing or decreasing the grating pitch will eliminate this condition. Also of note is that when the pitch becomes greater and much greater than the particle dimension for either particle, the scattering force remains constant at each position. While this was not true for the gradient force in the same situation (see

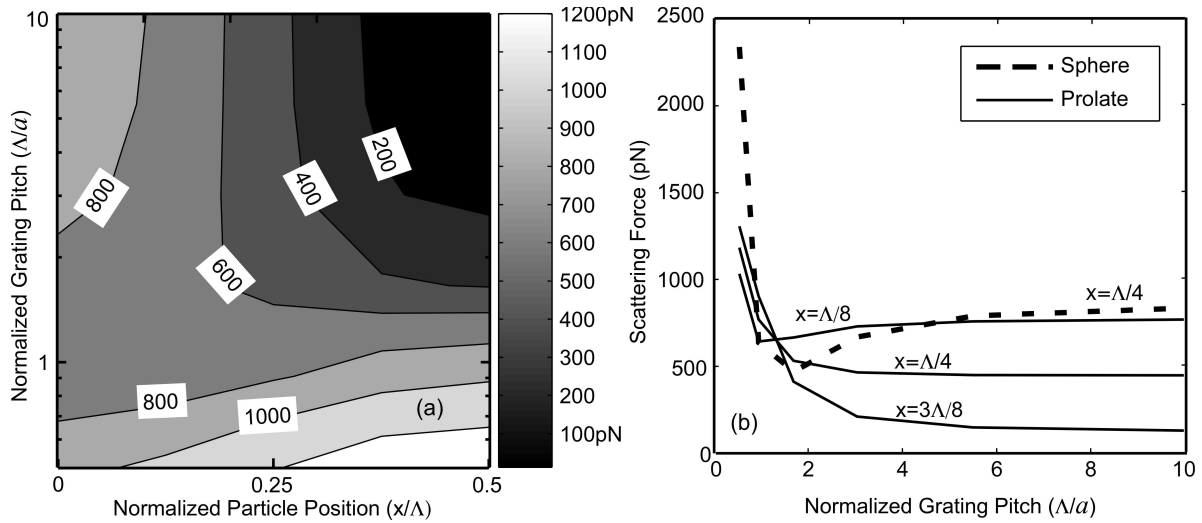


Figure 4. Scattering Force Induced by an Optical Landscape. (a) Contour plot of the scattering force on a prolate spheroid. Both the normalized grating pitch and particle position are varied. (b) Scattering force on a sphere at $x/\Lambda = 0.25$ and on a prolate spheroid at various positions.

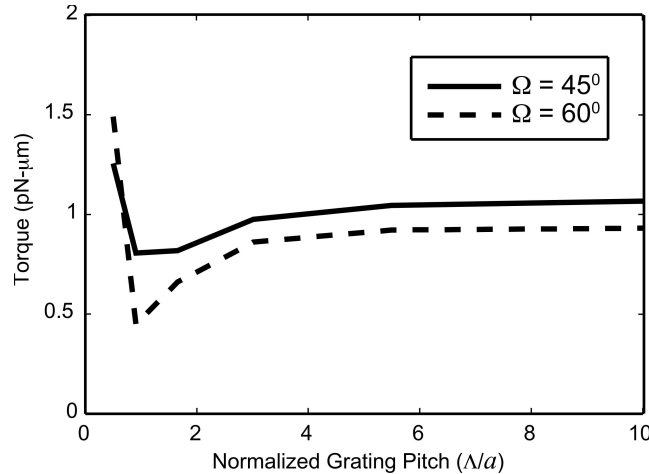


Figure 5. Total torque induced by an optical landscape on a prolate spheroid. The variable Ω refers to the angle between the positive \hat{x} -axis and the rotational axis of the particle.

Fig. 3(b)), the scattering force is not dependent on the intensity gradient between bright and dark fringes and, therefore, remains constant for a given electric field magnitude.

3.2.3 Total Torque

Two mechanisms of torque are present in optical landscapes: a gradient torque resulting from the intensity gradient across the particle, and a polarization-induced torque as discussed in Sec. 3.1. The total of these two torques is displayed in Fig. 5 for a prolate particle at position $x/\Lambda = 0.25$ and at two orientations measured from the positive \hat{x} -axis, $\Omega = 45^\circ$ and $\Omega = 60^\circ$. At small grating pitches, the gradient torque will dominate the characteristic as well as the magnitude of the total torque. As the grating pitch becomes larger, the intensity gradient across the particle becomes smaller, and the polarization-induced torque will dominate. We note that the ratio between the total torques of the two orientations at large values of Λ/a matches the ratio found in Fig. 2(b) for those same orientations. This is valid because for the optical landscape situation, TE polarization is used, meaning the parameter Ω is equal to the angle between the polarization orientation and the rotational

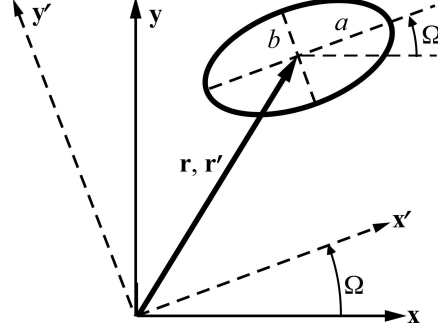


Figure 6. Coordinate systems used to represent a spheroidal particle at orientation Ω and position \mathbf{r}, \mathbf{r}' .

axis of the particle. All applicable parameters are the same for these two situations. The only difference is that here, an optical landscape is present rather than a single beam.

This result has far-reaching consequences in both theoretical and experimental study of particles with shape and their response in optical fields. As mentioned in the first section, most theoretical models neglect to include shape and instead focus only on spheres. Spherical particles will not experience a torque and many “real-world” particles are not perfectly spherical. As such, the overall response of the typical non-spherical particle will differ (at times greatly) from that predicted for a sphere. Therefore, a complete model must include the effects of gradient torques and polarization-induced torques on non-spherical particles.

4. THE FORM FACTOR MODEL

Our form-factor model has been described previously¹⁵ and will be briefly outlined here followed by a simple comparison to the T -matrix model. The heart of this model lies in the description of the form factor which contains information about the particle’s geometry and composition. A similar model was developed by Pelton et al⁶ for spherical particles. Because our initial derivation considers only spheroidal particles, we can write the form factor and all following equations in two dimensions with only two semi-diameters, a and b , where a is along the symmetry axis. Letting α represent the particle’s polarizability, we can write the form factor as

$$f[\mathbf{r}, \Omega] = \alpha\sqrt{ab} \exp\left\{-\frac{(x \cos \Omega + y \sin \Omega)^2}{2a^2} - \frac{(-x \sin \Omega + y \cos \Omega)^2}{2b^2}\right\}, \quad (14)$$

in the global coordinate system as defined in Fig. 6. Particle orientation is specified by Ω . The local coordinate system may also be used and is independent of orientation. Our fields of interest are periodic optical interference landscapes defined by Eq. (12) that, when convolved with the form factor, yield the force potential, V , and the optically-induced force, \mathbf{F} ,

$$V[\mathbf{r}, \Omega] = (f \circ I)[\mathbf{r}, \Omega] \quad (15a)$$

$$\mathbf{F}[\mathbf{r}, \Omega] = \int d\mathbf{F} d^3x = -\nabla V[\mathbf{r}, \Omega]. \quad (15b)$$

In a similar manner, the torque potential, \mathbf{A} , and optically-induced torque, \mathbf{M} , may be defined,

$$\mathbf{A}[\mathbf{r}, \Omega] = -(\mathbf{r}f \circ I)[\mathbf{r}, \Omega] \quad (16a)$$

$$\mathbf{M}[\mathbf{r}, \Omega] = \int ((\mathbf{x} - \mathbf{r}) \times d\mathbf{F}) d^3x = \nabla \times \mathbf{A}[\mathbf{r}, \Omega]. \quad (16b)$$

The general form of the spatially-varying optical force field has been defined previously⁶ while we offer that the spatially-varying optical torque field is a result of the optical landscape imparting a rotating force a distance \mathbf{x} from the particle position \mathbf{r} .

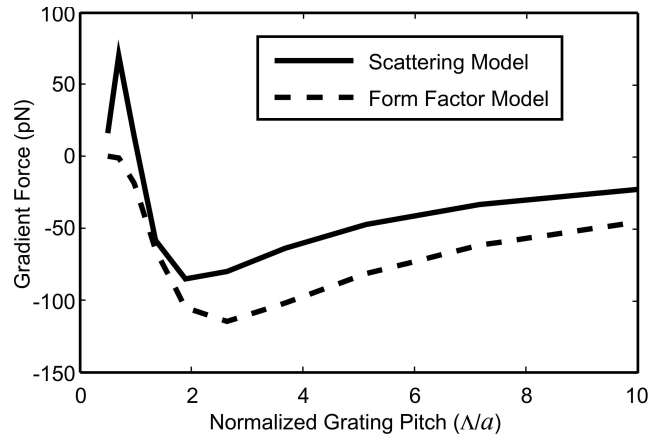


Figure 7. Gradient force on a prolate particle using optical scattering and form-factor models.

We submit that the form-factor model is significantly more straightforward in addition to requiring far less computational power to implement. While both of the models presented here can stand on their own, each is best suited for particular applications. The T -matrix model includes gradient-, scattering-, and polarization-induced effects, whereas the form-factor model considers only gradient-induced forces and torques. However, the form-factor model is easily suited for particles in a system where the medium is in a state of flow—a flow force is simply added to the hydrodynamic balance equation for force. The T -matrix model does not include motion or drag, thereby giving only instantaneous results in a system at rest. While both models are incomplete, together they promise to provide a much more complete view of how non-spherical particles behave in optical fields.

We provide a comparison of the two models' results for the gradient force on a prolate particle in Fig. 7. The orientation angle is $\Omega = 45^\circ$, the position is $\Lambda/a = 0.25$, and all other parameters are the same as described within results of the T -matrix model. Note that the trend is the same for both models and that the magnitudes for both are within an order of magnitude. These results lend credibility to the form-factor model since Maxwell stress tensor approaches and the T -matrix method are both well-known for their accuracy.

ACKNOWLEDGMENTS

The authors gratefully acknowledge support from a U.S. Department of Education GAANN Fellowship.

REFERENCES

- [1] Nieuwenhuis, J., Jachimowicz, A., Svasek, P., and Vellekoop, M., "Optimization of microfluidic particle sorters based on dielectrophoresis," *IEEE Sensors* **5**(5), 810–816 (2005).
- [2] Li, Y., Dalton, C., Crabtree, H. J., Nilsson, G., and Kaler, K. V. I. S., "Continuous dielectrophoretic cell separation microfluidic device," *Lab Chip* **7**(2), 239–48 (2007).
- [3] Wang, L., Flanagan, L. A., Monuki, E., Jeon, N. L., and Lee, A. P., "Dielectrophoresis switching with vertical sidewall electrodes for microfluidic flow cytometry," *Lab Chip* **7**(9), 1114–20 (2007).
- [4] Kim, U., Shu, C.-W., Dane, K. Y., Daugherty, P. S., Wang, J. Y. J., and Soh, H. T., "Selection of mammalian cells based on their cell-cycle phase using dielectrophoresis," *Proc. Natl. Acad. Sci. USA* **104**(52), 20708–12 (2007).
- [5] Vahey, M. D. and Voldman, J., "An equilibrium method for continuous-flow cell sorting using dielectrophoresis," *Anal. Chem.* **80**(9), 3135–43 (2008).
- [6] Pelton, M., Ladavac, K., and Grier, D., "Transport and fractionation in periodic potential-energy landscapes," *Phys. Rev. E* **70**(3), 10 (2004).
- [7] Lacasta, A. M., Sancho, J. M., Romero, A. H., and Lindenberg, K., "Sorting on periodic surfaces," *Phys. Rev. Lett.* **94**(16), 160601 (2005).

- [8] Cheong, F., Sow, C., Wee, A., Shao, P., Bettiol, A., Kan, J. V., and Watt, F., “Optical travelator: transport and dynamic sorting of colloidal microspheres with an asymmetrical line optical tweezers,” *Appl. Phys. B* **83**(1), 121–125 (2006).
- [9] Smith, R., Spalding, G., Dholakia, K., and MacDonald, M., “Colloidal sorting in dynamic optical lattices,” *J. Opt. A: Pure Appl. Opt.* **9**(8), S134–S138 (2007).
- [10] Roichman, Y., Wong, V., and Grier, D. G., “Colloidal transport through optical tweezer arrays,” *Phys. Rev. E* **75**(1 Pt 1), 011407 (2007).
- [11] Gleeson, J. P., Sancho, J. M., Lacasta, A. M., and Lindenberg, K., “Analytical approach to sorting in periodic and random potentials,” *Phys. Rev. E* **73**(4), 9 (2006).
- [12] Mu, W., Li, Z., Luan, L., Spalding, G., and Wang, G., “Force measurement on microspheres in an optical standing wave,” *J. Opt. Soc. Am. B* **25**(5), 763–767 (2008).
- [13] Bishop, A., Nieminen, T., Heckenberg, N., and Rubinsztein-Dunlop, H., “Optical application and measurement of torque on microparticles of isotropic nonabsorbing material,” *Phys. Rev. A* **68**(3), 033802 (2003).
- [14] Rockstuhl, C. and Herzig, H., “Calculation of the torque on dielectric elliptical cylinders,” *J. Opt. Soc. Am. A* **22**(1), 109–116 (2005).
- [15] Conover, B. and Escuti, M., “The response of particles with anisotropic shape within an optical landscape and laminar,” *Proc. SPIE* **6326**, 632614 (2006).
- [16] Mishchenko, M., “Far-field approximation in electromagnetic scattering,” *JQSRT* **100**(1-3), 268–276 (2006).
- [17] Nieminen, T., Rubinsztein-Dunlop, H., and Heckenberg, N., “Calculation and optical measurement of laser trapping forces on non-spherical particles,” *JQSRT* **70**(4-6), 627–637 (2001).
- [18] Simpson, S. H. and Hanna, S., “Optical trapping of spheroidal particles in gaussian beams,” *J. Opt. Soc. Am. A* **24**(2), 430–43 (2007).
- [19] Mishchenko, M. I., Travis, L. D., and Lacis, A. A., “Scattering, absorption, and emission of light by small particles,” (2002).
- [20] Escuti, M. J. and Crawford, G. P., “Holographic photonic crystals,” *Opt. Eng.* **43**(9), 1973 (2004).
- [21] Mishchenko, M., “Calculation of the amplitude matrix for a nonspherical particle in a fixed orientation,” *Appl. Opt.* **39**(6), 1026–1031 (2000).